Available online at www.sciencedirect.com
SCIENCE DIRECT®
Journal of Power Sources 115 (2003) 101–109
JOURNAL OF POWER SOURCES
www.elsevier.com/locate/jpowsour

Synthesis and charge–discharge properties of $LiNi_{1-x-y}Co_xM_yO_2$ (M = Al, Ga) compounds

Woo-Seong Kim[a], Kwang-il Chung[b], Yong-Kook Choi[b], Yung-Eun Sung[a,*]

[a]Department of Materials Science & Engineering, K-JIST, Kwangju 500-712, South Korea
[b]Department of Chemistry & RRC/HECS, Chonnam National University, Kwangju 500-757, South Korea

Received 19 August 2002; accepted 1 November 2002

Abstract

The synthesis and electrochemical characteristics of $LiNi_{1-x-y}Co_xM_yO_2$ (M = Al, Ga) compounds for use as positive-electrode (cathode) materials in rechargeable lithium batteries are investigated. Layered $LiNi_{1-x-y}Co_xM_yO_2$ is synthesized by solid-state reaction. The composition, structure, morphology, and particle size of the samples are characterized by means of inductively coupled plasma-atomic emission spectroscopy (ICP-AES), X-ray diffraction (XRD), thermal gravimetric analysis (TGA) and scanning electron microscopy (SEM). The electrochemical properties of $LiNi_{1-x-y}Co_xM_yO_2$ are examined by impedance spectroscopy and charge–discharge tests in half-cell and practical lithium batteries. The discharge capacities of the $LiNi_{1-x-y}Co_xM_yO_2$ compounds containing Al and Ga are above 190 mAh g^{-1}. Cells using these cathode materials show good low-temperature discharge and high-rate discharge performance, as well as good cycleability. The $LiNi_{0.8}Co_{0.18}Ga_{0.02}O_2$ compound, in particular, delivers approximately 210 mAh g^{-1} of discharge capacity with good reversibility.

Keywords: Cathode; Charge–dischage; Capacity; Lithium battery

1. Introduction

Rechargeable lithium batteries are used as the main power source in portable electronics, such as Personal Communication Services (PCSs), cellular phones, camcorders, and notebook PCs due to their specific energies, which are two or three times of those of nickel–cadmium (Ni–Cd) and nickel–metal hydride (Ni–MH) batteries. A need exists, however, for better performing rechargeable lithium batteries which are smaller in size, lightweight, have a higher capacity, and can be used with confidence [1–5]. Rechargeable lithium batteries are based on the use of intercalation compounds as electrodes in which lithium ions shuttle between the negative electrode (anode) and positive electrode (cathode) hosts. Layered $LiCoO_2$, $LiNiO_2$ and $LiMn_2O_4$ are candidate cathode materials for lithium-ion batteries and have been extensively investigated world-wide [4,6–13]. $LiNiO_2$, $LiCoO_2$, $LiMn_2O_4$ show higher operating voltages than layered chalcogenide materials. Currently, $LiCoO_2$ is being used as the cathode material in the majority of commercial lithium-ion batteries.

$LiCoO_2$ has several practical advantages in that the preparation of the electrode is easy to realize and the system is relatively safe. In addition, the material shows good reversibility and, compared with $LiNiO_2$, has a higher voltage-working region due to the Co^{3+}/Co^{4+} redox reaction. The specific energy of this system is also high. There are, however, some problems associated with $LiCoO_2$ electrode systems [13–17]. The discharge capacity of this system is approximately 155 mAh g^{-1}, which is only about half of its theoretical capacity of 274 mAh g^{-1}. The material is also toxic and expensive. By contrast, $LiMn_2O_4$ is inexpensive compared with other active materials, but its discharge capacity is low. As a result, many investigators have attempted to overcome this capacity problem [9,13,18,19].

The $LiNiO_2$ electrode has been shown to have high specific energy, long cycle-life, and low self-discharge [1,4,6,20–23]. The rechargeable capacity of active $LiNiO_2$ cathode material has been estimated to be near 170 mAh g^{-1}, which is significantly higher than that reported for $LiCoO_2$ and $LiMn_2O_4$. On the other hand, $LiNiO_2$ is unstable due to its electrochemical reactivity [24]. To solve this problem, investigations on mixed Ni–Co systems for batteries have been reported [24,25]. Further additives to $LiNiO_2$, such as V, Co, Mn, Ti, Ga, Al, to the cathode materials have been investigated and characterized in

* Corresponding author. Tel.: +82-62-970-2302; fax: +82-62-970-2304.
E-mail address: ysung@kjist.ac.kr (Y.-E. Sung).

0378-7753/02/$ – see front matter
PII: S0378-7753(02)00614-6

termsofelectrochemical and materials properties [15,24–27]. Nevertheless, the enhancement and role of these additives remain unclear, especially in the case of lithium batteries.

This study focuses on the synthesis of Al, Ga substituted $LiNi_{1-x-y}Co_xM_yO_2$ (M = Al, Ga) compounds as cathode materials to improve the capacity and stability of Ni–Co cathode systems. Inductively coupled plasma-atomic emission spectroscopy (ICP-AES), X-ray diffraction (XRD), thermal gravimetric analysis (TGA) and scanning electron microscopy (SEM) techniques are used to investigate the structure and shape of the $LiNi_{1-x-y}Co_xM_yO_2$ compounds. The electrochemical characteristics of electrode materials are studied by means of impedance spectroscopy and charge–discharge tests in half cells and rechargeable lithium batteries.

2. Experimental

The $LiNi_{1-x-y}Co_xM_yO_2$ (M = Al, Ga) compounds were synthesized via a solid-state reaction of precursors of $LiOH{\cdot}H_2O$ (99.95%, Aldrich), NiO (Aldrich), CoO (Aldrich) and other materials with molar ratios of Li:(Ni + Co + M) from 1.06. The starting materials were chemically analyzed for lithium and Ni + Co + Ga or Al, respectively, in order to determine the Li:(Ni + Co) ratio in the reaction mixture. The reactions were mixed thoroughly by ball-milling and then pressed into pellets. The pellets were sintered at 650 °C in oxygen for 48 h. These pellets were used for characterization or alternatively, powdered for battery tests.

Elemental analyses of the synthesized $LiNi_{1-x-y}Co_xM_yO_2$ samples were performed by means of the ICP–AES method (JY plus). The structure of the $LiNi_{1-x-y}Co_xM_yO_2$ samples was characterized by X-ray diffraction on a Rint 2000 wide-angle Goniometer with Cu Kα radiation at 32 kV and 40 mA. A simultaneous thermal analyzer (STA1640) was employed to determine the thermal behaviour of $LiNi_{1-x-y}Co_xM_yO_2$ in a temperature range between room temperature and 1000 °C. Electron micrographs of the samples were obtained with a JSM-5400 Scanning Electron Microscope (NORAN Instruments).

The specific capacity of the materials was measured for two different cell arrangements. One was an open cell. In this case, a half cell versus metallic lithium was prepared using an electrolyte mixture of ethylene carbonate (EC)/dimethyl carbonate (DMC) in a 3:7 ratio with 1 M $LiPF_6$. The other arrangement was a unique ICR18650 cylindrical cell. Kawasaki Mesophase Fine Carbon (KMFC) was used for the anode electrode. The standard charge and discharge rates were each C/9. The measured voltage range was from 2.5 to 4.2 V versus Li/Li^+. For a more detailed investigation, an open cell was used in argon-filled glove box. The reference and counter electrodes were metallic lithium. The active material was pressed to on an aluminum foil. In both cases, the cathode electrode was a mixture of active material (91 wt.%), conducting material (carbon black 6 wt.%) and binder (PVDF 3 wt.%). Samples were investigated in an organic electrolyte system. High purity $LiPF_6$/EC + DMC (Mitsubishi Chemical, Battery grade) was used as the electrolyte solution. The properties of the $LiNi_{1-x-y}Co_xM_yO_2$ and the intercalation of $LiNi_{1-x-y}Co_xM_yO_2$ through the passivation film were investigated by means of ac impedance spectroscopy and a Potentionstat/Galvanostat (Autolab). The cycling tests of the electrode and battery systems were carried out with a TOYO battery cycle system (Model HRC6064A). For capacity measurements, the typical constant-current mode was used.

3. Results and discussion

The ICP-AES analysis for $LiNi_{1-x-y}Co_xM_yO_2$ is summarized in Table 1. The concentrations were obtained using ICP-AES and the composition of compounds was calculated from the ratio of the concentrations. The results are in agreement with the calculated compositions during synthesis within the limits of error. The compositions of the synthesized $LiNi_{1-x-y}Co_xM_yO_2$ samples were determined to be $LiNi_{0.8}Co_{0.2}O_2$, $LiNi_{0.81}Co_{0.16}Al_{0.03}O_2$, $LiNi_{0.8}Co_{0.18}Ga_{0.02}O_2$. The homogeneous region of $Li_xCo_{2-x}O_2$ is known to be $x > 0.98$, but $1 > x > 0.6$ in $Li_xNi_{2-x}O_2$. The variation in the $Li_xNi_{2-x}O_2$ homogeneous region is relatively large and as a result stochiometric synthesis of $LiNiO_2$ is difficult. Therefore, structural analysis was performed using the X-ray diffraction technique.

X-ray diffraction patterns of synthesized $LiNi_{1-x-y}Co_xM_yO_2$ compounds are shown in Fig. 1. All diffraction lines can be indexed by assuming the structure to be a hexagonal lattice of the α-$NaFeO_2$ type. The lattice parameters of $LiNi_{0.8}Co_{0.18}Ga_{0.02}O_2$ viz., $a = 2.866$ Å and $c = 14.164$ Å are in good agreement with previously reported values [24]. As can be seen in Fig. 1, the separations of the (0 0 3) plane, d_{003}, of $LiNi_{0.8}Co_{0.2}O_2$, $LiNi_{0.81}Co_{0.16}Al_{0.03}O_2$, and $LiNi_{0.8}Co_{0.18}Ga_{0.02}O_2$ are similar to each other with $2\theta = 18.8$, 18.8, and 18.82°, respectively. The d_{104} values are also similar with $2\theta = 44.6$, 44.5 and 44.69°, respectively. Overall, no clear structure differences are found as the results of the addition of small amount of Al or Ga to $LiNi_{0.8}Co_{0.2}O_2$. The intensity ratio of the (0 0 3) and (1 0 4) peaks has been used as a population

Table 1
ICP-AES data for $LiNi_{1-x-y}Co_xM_yO_2$ compounds synthesized by solid-state reaction

Sample	Concentration (wt.%)				
	Li	Ni	Co	Ga	Al
$LiNi_{0.8}Co_{0.2}O_2$	7.07	47.83	11.98	–	–
$LiNi_{0.8}Co_{0.18}Ga_{0.02}O_2$	7.07	48.02	10.91	1.40	–
$LiNi_{0.81}Co_{0.16}Al_{0.03}O_2$	7.19	49.02	9.79	–	0.82

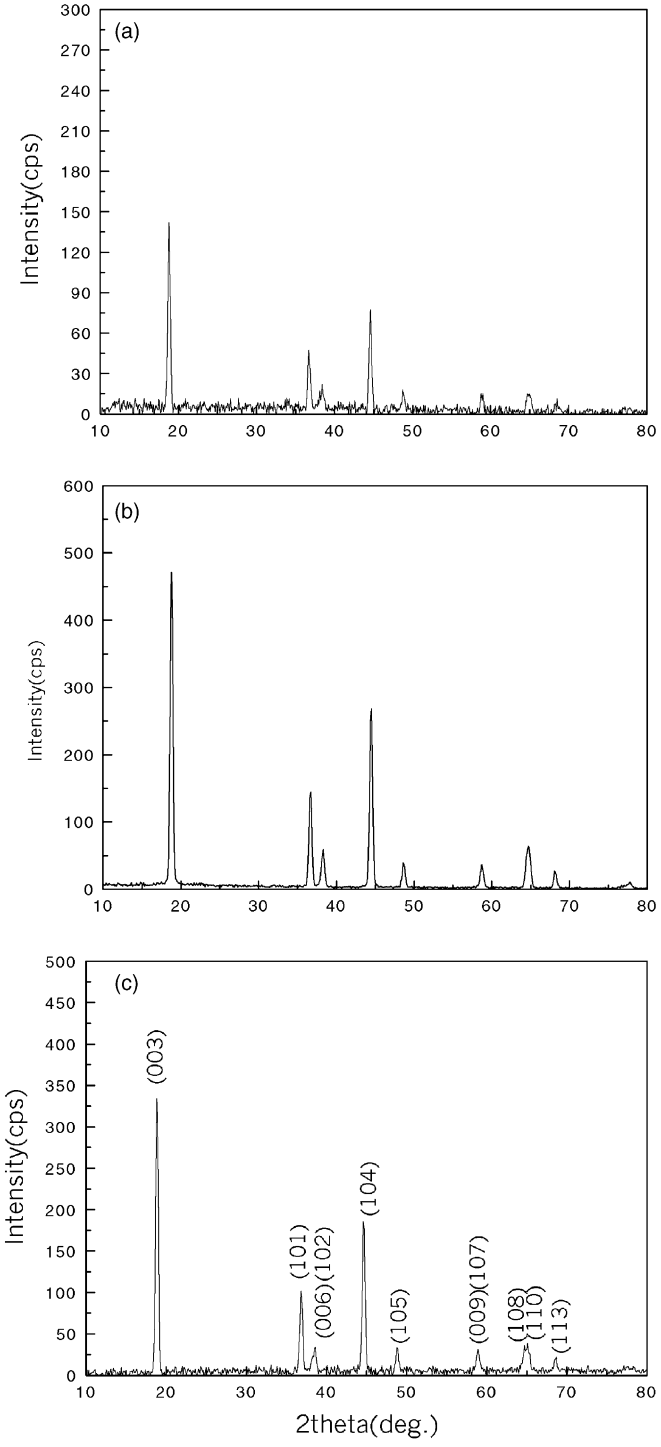

Fig. 1. XRD patterns of (a) $LiNi_{0.8}Co_{0.2}O_2$, (b) $LiNi_{0.81}Co_{0.16}Al_{0.03}O_2$, and (c) $LiNi_{0.8}Co_{0.18}Ga_{0.02}O_2$.

level by the phase of $LiNiO_2$, i.e. the degree of cation mixing, since the intensity of (0 0 3) peaks is affected by 3*a*, 3*b* site exchange of Li and Ni, but that of (1 0 4) peaks is not [10]. In general, the reversible capacity is known to decrease when $I(0\,0\,3):I(1\,0\,4) < 1.2$ and is completely inactive when $I(0\,0\,3):I(1\,0\,4) < 1.0$ [13,23,24]. In these sample, the ratios of $I(0\,0\,3):I(1\,0\,4)$ are 1.71, 1.76 and 1.79 for $LiNi_{0.8}Co_{0.2}O_2$, $LiNi_{0.81}Co_{0.16}Al_{0.03}O_2$, and $LiNi_{0.8}Co_{0.18}Ga_{0.02}O_2$, respectively. Obviously, the values are well above 1.2. Therefore, these samples are all well crystallized. The ratio of $I(0\,0\,3):I(1\,0\,4)$ is highest for $LiNi_{0.8}Co_{0.18}Ga_{0.02}O_2$. Therefore, the discharge capacity of $LiNi_{0.8}Co_{0.18}Ga_{0.02}O_2$, which has an electrochemically higher active crystalline content, is expected to be higher than the others.

The thermal behaviour of the $LiNi_{1-x-y}Co_xM_yO_2$ compounds was determined by TGA analysis. The results are shown in Fig. 2, all samples were measured at a sweep rate of 5 °C per min. Significant changes to the weight-loss profile are found as the compounds become altered. Within a temperature range of up to 1000 °C, the weights of the samples decrease continuously, which can be attributed to the decomposition of $LiNi_{1-x-y}Co_xM_yO_2$. Small weight losses near 200–300 °C are due to the release of water. Thus, the samples were dried at 220 °C before mixing for electrodes. Weight losses measured using TGA at about 690–730 °C are found to be almost entirely due to the loss of oxygen [23]. The addition of Ga to $LiNiCoO_2$, viz., $LiNi_{0.8}Co_{0.18}Ga_{0.02}O_2$, decreases the onset temperature of oxygen loss. Consequently, the synthesis and sintering were performed in an oxygen atmosphere to suppress any evolution of oxygen.

Scanning electron microscopy (SEM) was used to investigate the morphology of synthesized $LiNi_{1-x-y}Co_xM_yO_2$ powders. Electron micrographs of the $LiNi_{1-x-y}Co_xM_yO_2$ compounds are shown in Fig. 3. The particle shapes of $LiNi_{1-x-y}Co_xM_yO_2$ and $LiNi_{0.8}Co_{0.18}Ga_{0.02}O_2$ are largely spherical. By contrast, the structure of $LiNi_{0.8}Co_{0.18}Ga_{0.02}O_2$ is more prismatic. Overall, the particle sizes of $LiNi_{1-x-y}Co_xM_yO_2$ samples are about 1–15 μm. Capacity of performance are known to be better when electrode materials are smaller in size. $LiNi_{1-x-y}Co_xM_yO_2$ compounds, however, no noticeable differences in size.

Impedance spectra were measured after an Li^+ intercalation–de-intercalation reaction over a frequency range from 100 kHz to 0.01 Hz. Typical Nyquist plots for $LiNi_{0.8}Co_{0.18}Ga_{0.02}O_2$ at equilibrium after (a) initial Li^+ de-intercalation and (b) intercalation in an open cell are presented in Fig. 4. The data are combinations of a depressed semicircle at high-to-medium frequencies with a Warburg-type element at the low frequencies. A typical impedance diagram for a practical Li battery using $LiNi_{0.8}Co_{0.18}Ga_{0.02}O_2$ is shown in Fig. 4(c). Interpretation of the impedance spectra is based on the equivalent circuit shown in Fig. 4(d). The symbols R_{sol}, R_f, R_{ct}, C_f, C_{dl}, and Z_w, denote the solution resistance, film resistance, charge-transfer resistance, capacitance of the electrolyte/film, capacitance of the film/electrode surface, and Warburg impedance, respectively. The high-frequency semicircle, the medium-frequency semicircle, and the sloping line at low frequency can be attributed to Li^+ migration through the film, that covers the electrode surface, the Li^+ charge-transfer in the film/electrode interface and the solid-state diffusion of Li^+ in the electrode layer, respectively. To measure the charge-transfer resistance, a

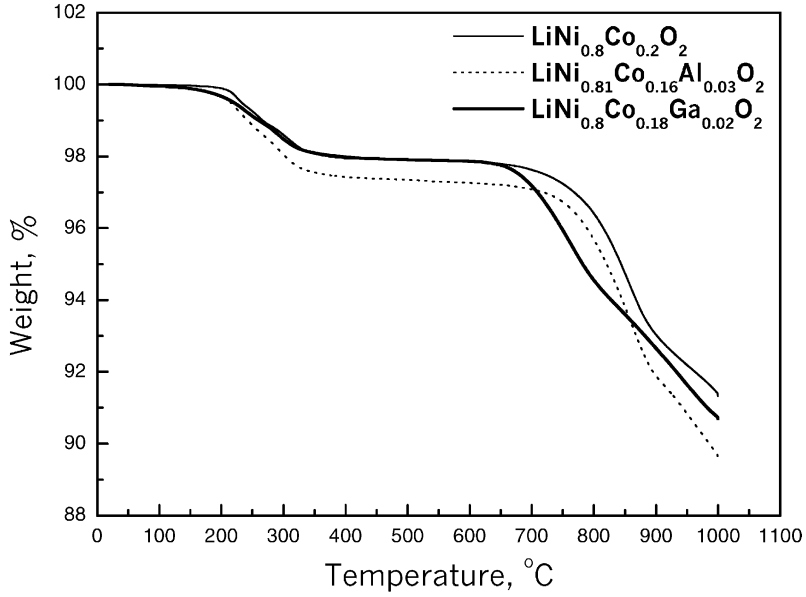

Fig. 2. TGA curves for $LiNi_{0.8}Co_{0.2}O_2$, $LiNi_{0.81}Co_{0.16}Al_{0.03}O_2$, and $LiNi_{0.8}Co_{0.18}Ga_{0.02}O_2$.

non-linear-least-squares fitting (NLLS fitting) program was used. The charge transfer resistance of $LiNi_{0.8}Co_{0.18}Ga_{0.02}O_2$ is around 50 Ω. This value is similar to previously reported values for $LiNiO_2$ [23]. As shown in Fig. 4(a) and (b), only one semicircle eventuates from the overlapping R_f and R_{ct}, which indicates the dominance of R_{ct}. This indicates that the redox reaction of Li^+ is hindered between the solutions of film. The data in Fig. 4(c) show a low resistance in a practical cell due to reduced film resistance and enhanced electron transfer between the film and the current-collector during cell fabrication. The resistance, 20 mΩ, is comparable with the resistance of the solution itself.

In order to compare the electrochemical performance of $LiNi_{1-x-y}Co_xM_yO_2$ materials, the initial discharge capacity of $LiNi_{1-x-y}Co_xM_yO_2$ cells was measured. Discharge tests of KMFC/$LiNi_{1-x-y}Co_xM_yO_2$ cells were carried out in the voltage range 3.0–4.2 V at a constant current of 0.68 mA cm^{-2} after formation at a constant current density of 1.06 mA cm^{-2}. Typical discharge profiles of $LiNi_{1-x-y}Co_xM_yO_2$ samples are shown in Fig. 5. The discharge capacity of $LiNi_{0.8}Co_{0.2}O_2$ is 179 mAh g^{-1} and is higher than that of pure $LiNiO_2$ or $LiCoO_2$. This capacity is lower, however, than 191 mAh g^{-1} for $LiNi_{0.81}Co_{0.16}Al_{0.03}O_2$ and 210 mAh g^{-1} for $LiNi_{0.8}Co_{0.18}Ga_{0.02}O_2$. The working voltages were 3.9 V for $LiNi_{0.8}Co_{0.18}Ga_{0.02}O_2$ and 3.7 V for $LiNi_{0.8}Co_{0.2}O_2$ and $LiNi_{0.81}Co_{0.16}Al_{0.03}O_2$, respectively. By contrast, $LiNi_{1-x-y}Co_xM_yO_2$ samples displayed much better electrochemical properties, with discharge capacities of 175–210 mAh g^{-1}. In particular, $LiNi_{0.8}Co_{0.18}Ga_{0.02}O_2$ electrode gave the highest discharge capacity. The reason for this is the addition of Ga^{3+}, which acts as the axis of the crystalline phase. It is expected that the phase separation will be inhibited by a uniform Li^+ distribution and a restriction in Li^+ rearrangement at a deeply charged state. To achieve this condition an attempt was made to achieve a uniform substitution of Ni^{3+} using the trivalent ion, the valence of which does not vary. Li^+ di-intercalation requires a valence change in the nickel ion from 3+ to 4+, therefore Li^+ ions will remain around the substituted ion and be distributed uniformly at a deeply charged state. Furthermore, the Li^+ rearrangement will be restricted by restraining Li^+ around the substituted ion. The dopant Ga ion substitutes for the nickel ion, in that it forms a trivalent Ga^{3+} ion, and its ionic radius (0.76 Å). Moreover, the Ga^{3+} ion acts as a fixed cation. If Ni^{3+} ion in charging is changed Ni^{4+} it forms NiO_2. On the other hand, if Ga^{3+} ion exchanges for Ni^{3+} ion, Ga^{3+} ion is fixed in the structure and permits the free charge/discharge of Ni^{3+}/Ni^{4+}.

The discharge capability of KMFC/$LiNi_{1-x-y}Co_xM_yO_2$ cells was studied at various temperature, viz., −20, 0, 20, 40, 60 °C. The resulting discharge profiles are shown in Fig. 6 as a function of temperature. The discharge capacities slowly decrease from 60 to 0 °C, then abruptly fall as the temperature is decreased further. This indicates that the activities of these materials decrease with decreasing temperature. Generally, Ni–Cd and Ni–MH batteries using aqueous electrolytes show 60% of the capacity ratio for 0/20 °C and 40% of the ratio for −20/20 °C. This is due to an abrupt decrease in electrochemical activities below the freezing temperature of water in aqueous electrolyte. A lithium rechargeable battery, however, require > 80% to achieve a capacity ratio of −20/20 °C. In $LiNi_{1-x-y}Co_xM_yO_2$ cells, the ratios of −20/20 °C are above 85%. The low-temperature effect for these materials could be an important advantage in practical battery systems. In the case of Al-substituted material, the working voltage is higher than for the other compounds. This result is in good agreement with previous results [28].

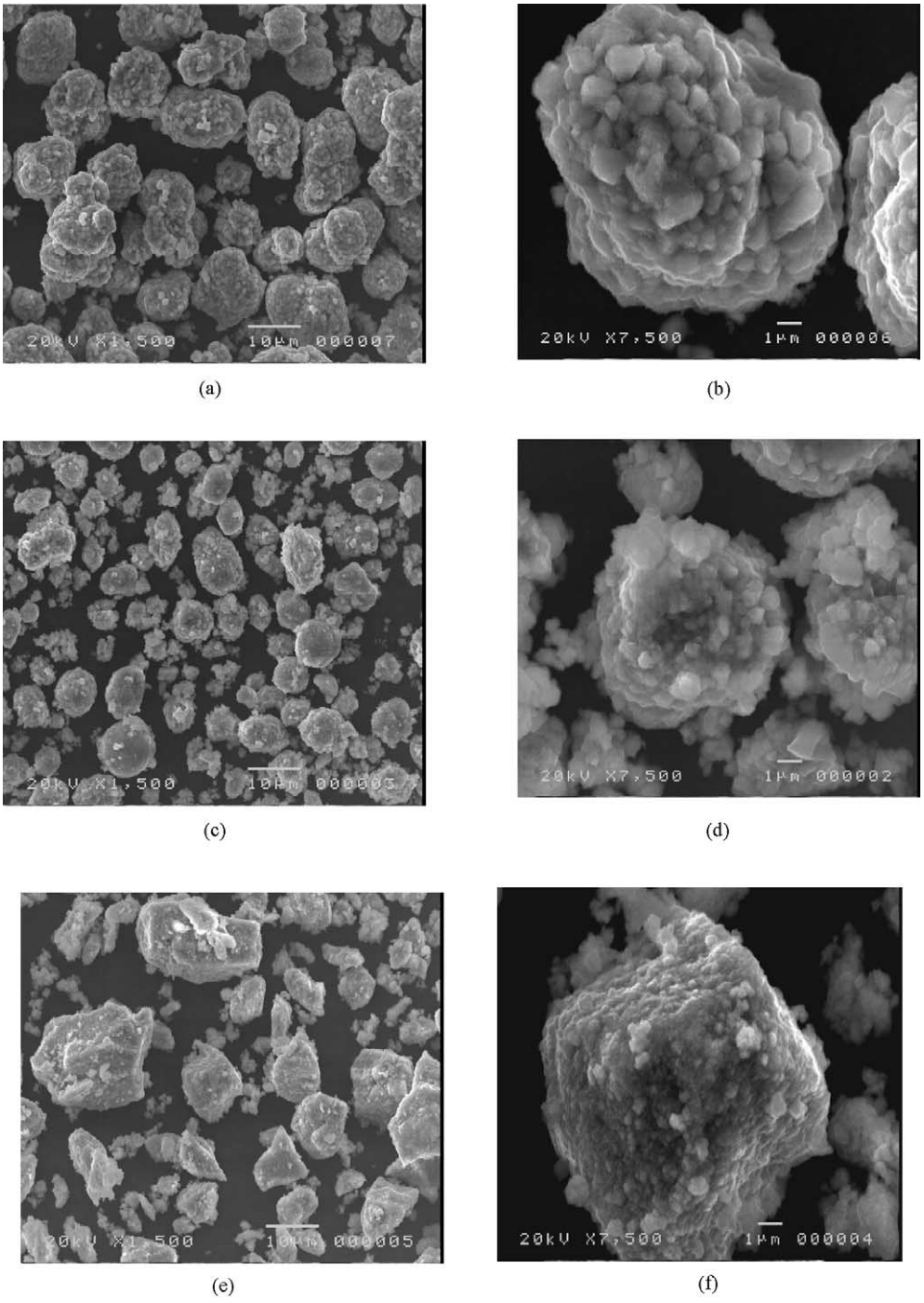

Fig. 3. SEM micrograph of $LiNi_{1-x-y}Co_xM_yO_2$ after heat treating the precursors to 600 °C for 2 h. (a, b) $LiNi_{0.8}Co_{0.2}O_2$; (c, d) $LiNi_{0.81}Co_{0.16}Al_{0.03}O_2$; (e, f) $LiNi_{0.8}Co_{0.18}Ga_{0.02}O_2$ (a, c, e) 1500× and (b, d, f) 7500×.

The discharge rate capability was studied using a KMFC/$LiNi_{1-x-y}Co_xM_yO_2$ cell. The discharge profiles at rates of 0.2, 0.5, 1.0 and 2.0 CmA are given in Fig. 7. The discharge capacity and working voltage both decrease with increasing current density. Generally, more than 80% is required for the ratio of the discharge capacities at 2 and 0.2 CmA. All cells using these $LiNi_{1-x-y}Co_xM_yO_2$ electrodes show good ratios that are higher than 90%. The discharge rate capability of the $LiNi_{0.81}Co_{0.16}Al_{0.03}O_2$ and $LiNi_{0.8}Co_{0.18}Ga_{0.02}O_2$ electrodes, in particular, are better than that of $LiNi_{0.8}Co_{0.8}O_2$.

Cycling stability is an important and desirable feature in most secondary battery applications. The $LiNi_{1-x-y}Co_xM_yO_2$ system exhibits excellent cycling stability and a high reversible capacity. Cycle-life plots of $LiNi_{1-x-y}Co_xM_yO_2$ electrodes are presented in Fig. 8. The cell voltage

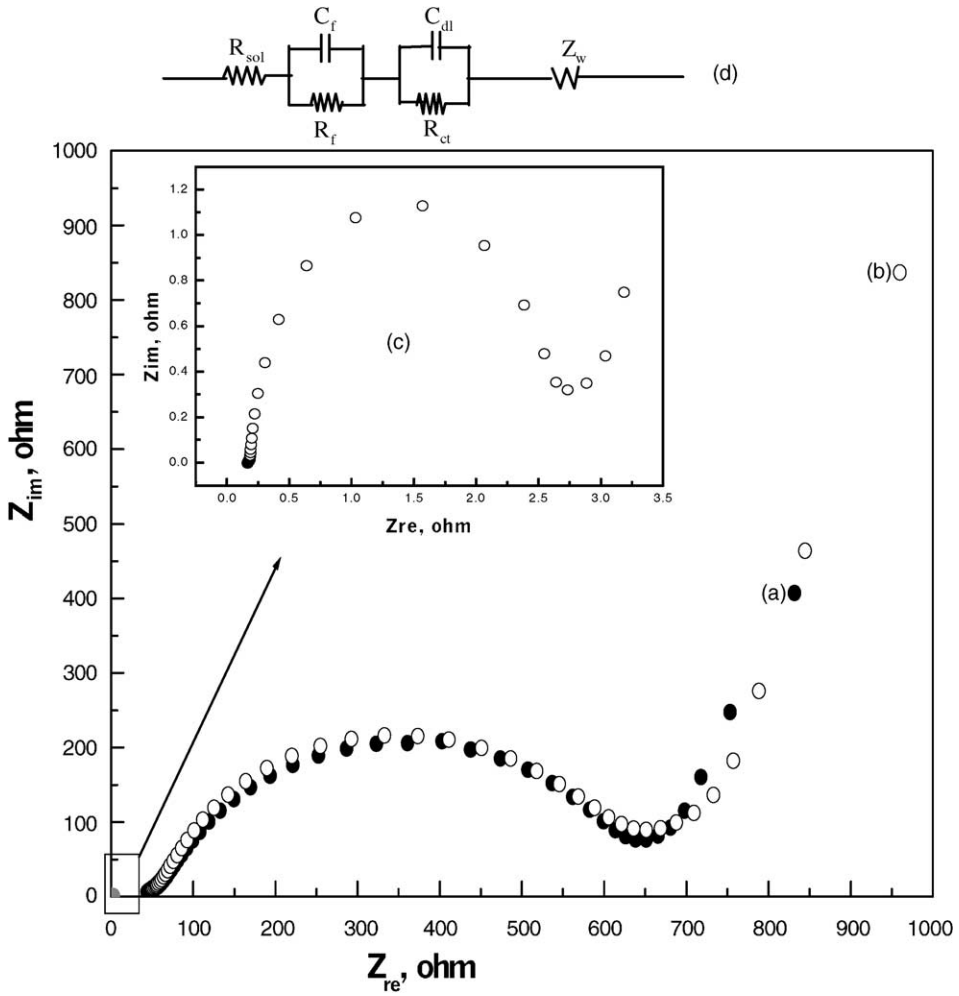

Fig. 4. The ac impedance spectra of $LiNi_{0.8}Co_{0.18}Ga_{0.02}O_2$ electrode in 1 M $LiPF_6$/EC:DEC(1:1): (a) after charge, (b) after discharge, (c) after charge for a practical cell, and (d) imaginary impedance circuit.

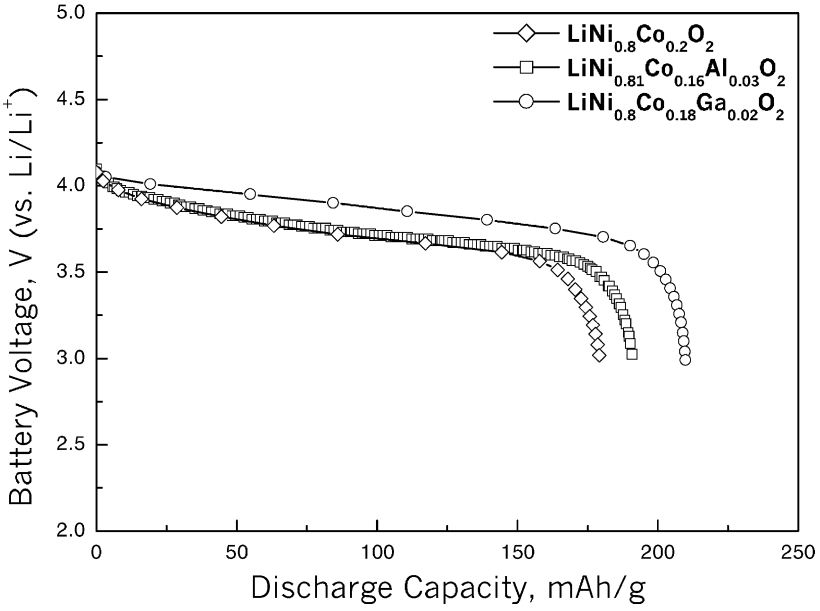

Fig. 5. Discharge curves of $LiNi_{0.8}Co_{0.2}O_2$, $LiNi_{0.81}Co_{0.16}Al_{0.03}O_2$, and $LiNi_{0.8}Co_{0.18}Ga_{0.02}O_2$ in 1 M $LiPF_6$/EC:DEC (1:1) with a current density of 0.68 mA/cm^2. Lithium metal was used as the anode.

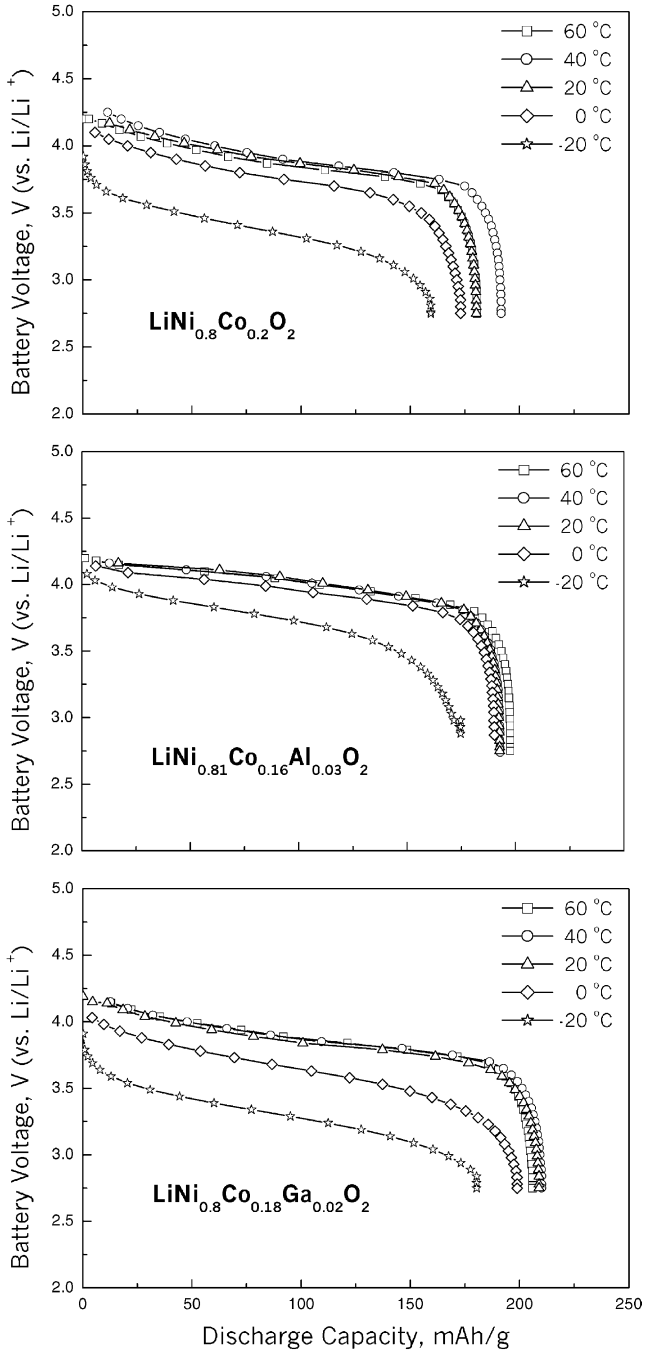

Fig. 6. Discharge profiles of $LiNi_{0.8}Co_{0.2}O_2$, $LiNi_{0.81}Co_{0.16}Al_{0.03}O_2$, and $LiNi_{0.8}Co_{0.18}Ga_{0.02}O_2$ in 1 M $LiPF_6$/EC:DEC(1:1) at various temperatures. The temperatures were −20, 0, 20, 40, and 60 °C. The anode was KMFC electrode. The charge condition was 0.5 CmA, 4.2 V-limited, and 3 h, and discharge was 0.2 CmA and 3.0 V cut-off.

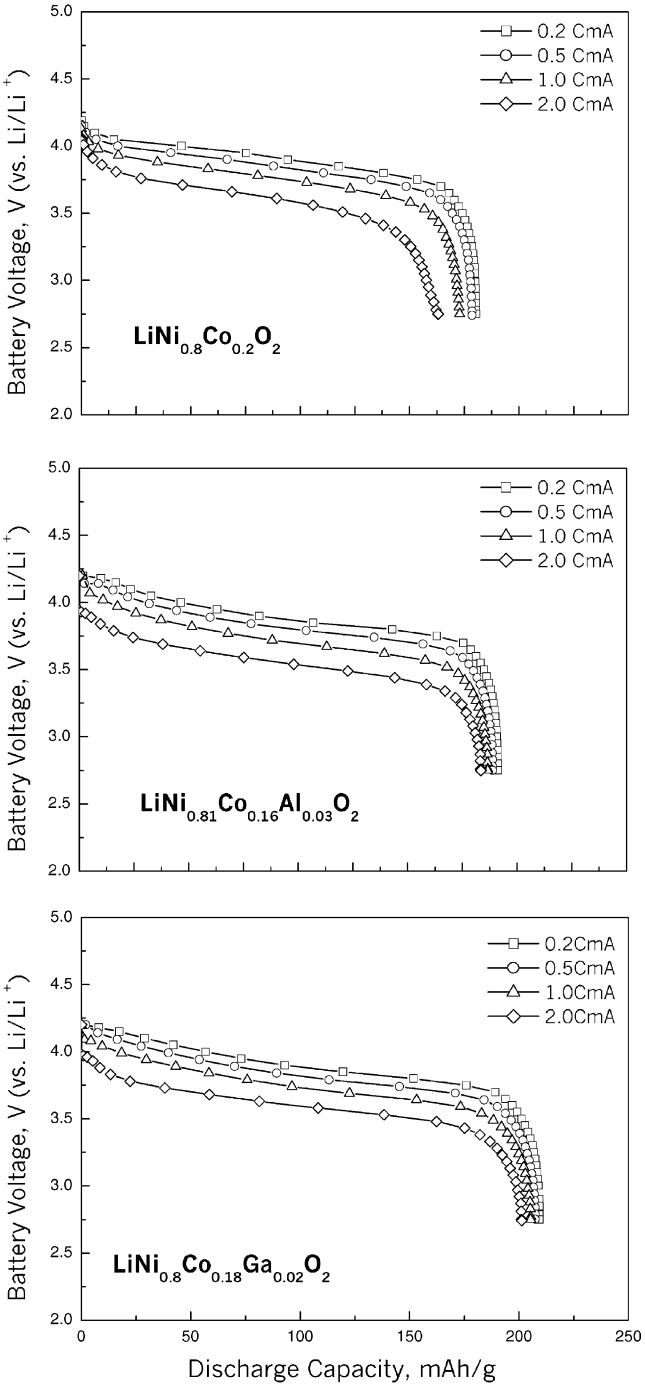

Fig. 7. Discharge profiles of $LiNi_{0.8}Co_{0.2}O_2$, $LiNi_{0.81}Co_{0.16}Al_{0.03}O_2$, and $LiNi_{0.8}Co_{0.18}Ga_{0.02}O_2$ in 1 M $LiPF_6$/EC:DEC(1:1) at various rates. The rates were 0.2, 0.5, 1.0, and 2.0 CmA. The anode was KMFC electrode. The charge condition was 0.5 CmA, 4.2 V-limited, and 3 h.

is cycled between 4.2 and 3.0 V. $LiNi_{0.8}Co_{0.18}Ga_{0.02}O_2$ displays the best electrochemical activity delivering an initial charge capacity of 238 mAh g^{-1} and discharge capacity of 210 mAh g^{-1}. During the first cycle, about 28 mAh g^{-1} of the specific capacity is the irreversible portion. From the second cycle onwards, the reversibility of the electrode is quite excellent. After 30 cycles, the electrode still delivers 190 mAh g^{-1} of specific discharge capacity at a rate of capacity loss of 0.093% per cycle. By comparison, the rate of capacity loss in $LiNi_{0.8}Co_{0.2}O_2$ and $LiNi_{0.81}Co_{0.16}Al_{0.03}O_2$ is 0.1128 and 0.1456% per cycle. After 300 cycles, the discharge capacities of $LiNi_{0.8}Co_{0.2}O_2$, $LiNi_{0.81}Co_{0.16}O_2$ and $LiNi_{0.8}Co_{0.18}Ga_{0.02}O_2$ are 130, 139 and 160 mAh g^{-1}, respectively.

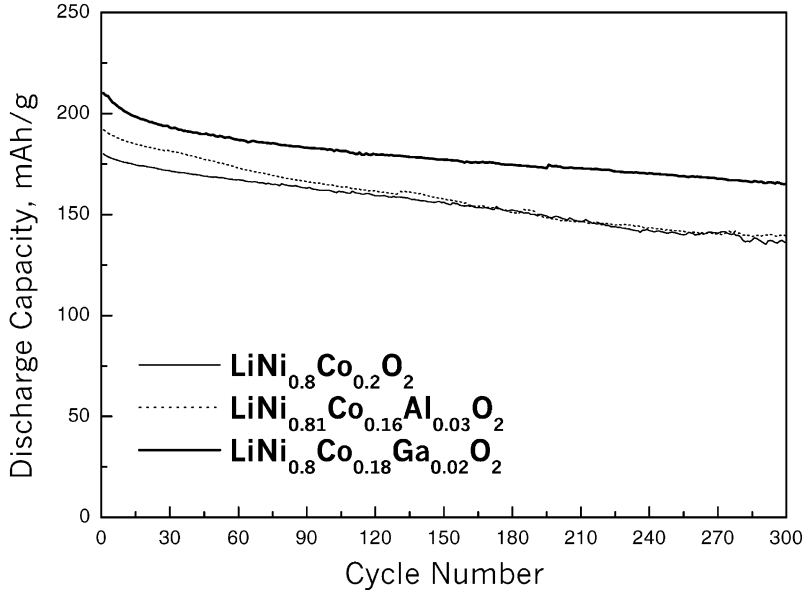

Fig. 8. Discharge capacities versus cycle numbers of $LiNi_{0.8}Co_{0.2}O_2$, $LiNi_{0.81}Co_{0.16}Al_{0.03}O_2$, and $LiNi_{0.8}Co_{0.18}Ga_{0.02}O_2$. The cell type was cylindrical 18650. The charge condition was 0.5 CmA, 4.2 V-limited, and 2.5 h, and discharge was 0.5 CmA and 3.0 V cut-off.

Table 2
Data for $LiNi_{1-x-y}Co_xM_yO_2$ cells

	$LiNi_{0.8}Co_{0.2}O_2$	$LiNi_{0.81}Co_{0.16}Al_{0.03}O_2$	$LiNi_{0.8}Co_{0.18}Ga_{0.02}O_2$
Discharge capacity (mAh g^{-1})	179.13	190.77	209.95
Discharge capacity ratio [(−20 °C/20 °C)100%]	88.41	90.66	86.36
Discharge capacity ratio [(2 CmA/0.2 CmA)100%]	90.39	96.00	96.12
Cycleability (rate of discharge loss per cycle)	0.1128	0.1456	0.0936

4. Conclusion

The nature and electrochemical characteristics of $LiNi_{1-x-y}Co_xM_yO_2$ (M = Al, Ga) compounds as a cathode for rechargeable lithium batteries has been investigated. The discharge capacity of $LiNi_{1-x-y}Co_xM_yO_2$ compounds was above 170 mAh g^{-1}. An $LiNi_{1-x-y}Co_xM_yO_2$ compound which contains Ga was found to be capable of delivering about 210 mAh g^{-1} discharge capacity with good reversibility. The characteristics for these cathode materials are summarized in Table 2. The initial coulomb efficiencies are 88 and 90%, i.e. similar to that of a practical battery. Initial discharge capacities are 179, 191 and 210 mAh g^{-1} for $LiNi_{0.8}Co_{0.2}O_2$, $LiNi_{0.8}Co_{0.16}Al_{0.03}O_2$, $LiNi_{0.8}Co_{0.18}Ga_{0.02}O_2$. The capacities are higher than 155 mAh g^{-1} of $LiCoO_2$ or 130 mAh g^{-1} of $LiMn_2O_4$. Low temperature discharge effects and high-rate discharge effects, which are important determinants of the characteristics of a battery system, are also excellent. In addition, the rate of capacity loss per cycle is less than 0.1% for the addition of Ga to $LiNi_{1-x-y}Co_xM_yO_2$.

Acknowledgements

This work was supported by the Ministry of Commerce, Industry and Energy and by the Brain Korea 21 Project from the Ministry of Education in Korea. One author (YKC) acknowledges funding from the RRC-HECS of Chonnam National University.

References

[1] J.R. Dahn, U. von Sacken, M.W. Juzkow, H. Al-Jannaby, J. Electrochem. Soc. 138 (1991) 2207.
[2] C. Delmas, I. Saadoune, Solid-States Ionics 53–56 (1992) 370.
[3] K.M. Abaraham, Electrochem Acta 38 (1993) 1233.
[4] H. Noguchi, T. Miyashita, K. Yamato, M. Yoshio, Denki Kagaku 61 (1993) 720.
[5] T. Ohzuku, A. Ueda, Solid-State Ionics 69 (1994) 201.
[6] J.R. Dahn, U. von Sacken, C.A. Michal, Solid-States Ionics 44 (1990) 87.
[7] T. Ohzuku, A. Ueda, M. Nagayama, J. Electrochem. Soc. 140 (1993) 1862.
[8] C. Delmas, H. Cognac-Aurodou, J.M. Cocciantell, M. Menetrier, J.P. Doumerc, Solid-State Ionics 69 (1994) 257.
[9] Y. Xia, M. Yoshio, J. Power Sources 63 (1996) 97.
[10] Y.-M. Choi, S.-I. Pyun, S.-I. Moon, Y.-E. Hynug, J. Power Sources 72 (1998) 83.
[11] P.N. Kumta, D. Gallet, A. Waghray, G.E. Blomgren, M.P. Setter, J. Power Sources 72 (1998) 91.
[12] M. Okada, Y.S. Lee, M. Yosio, J. Power Sources 90 (2000) 196.
[13] D. Aurbach, K. Gamolsky, B. Markovsky, G. Salitra, Y. Gofer, U. Heider, R. Oesten, M. Schmidt, J. Electrochem Soc. 147 (2000) 1332.
[14] C. Delmas, I. Saadoune, J. Power Sources 43-44 (1993) 595.

[15] A. Ueda, T. Ohzuku, J. Electrochem. Soc. 141 (1994) 2010.
[16] T. Nohma, H. Kurkawa, M. Uehara, M. Takahashi, K. Nishio, T. Sailo, J. Power Sources 54 (1995) 522.
[17] X. Xi, G. Zaiping, N. Yanna, J. New Mat. Electrochem. Systems 3 (2000) 327.
[18] J.-H. Choy, D.-H. Kim, C.-W. Kwon, S.-J. Hwang, Y.-I. Kim, J. Power Sources 77 (1999) 1.
[19] M.M. Doeff, A. Anapolsky, L. Edman, T.J. Richardson, L.C.D. Jonghe, J. Electrochem. Soc. 148 (2001) A230.
[20] W. Li, I.N. Reimers, J.R. Dahn, Solid-State Ionics 67 (1993) 123.
[21] T. Miyashita, H. Noguchi, K. Yamato, M. Yoshio, J. Ceram. Soc. Jpn. 102 (1994) 259.
[22] R. Moshtev, P. Zlatilova, V. Manev, K. Tagawa, J. Power Sources 62 (1996) 59.
[23] G.X. Wang, S. Zhong, D.H. Bradhurst, S.X. Dou, H.K. Liu, J. Power Sources 76 (1998) 141.
[24] T. Ohzuku, A. Ueda, M. Nagayama, Y. Iwakoshi, H. Komori, Electrochim. Acta 38 (1993) 1159.
[25] H. Arai, S. Okada, Y Sakurai, J. Yamaki, J. Electrochem. Soc. 144 (1997) 3117.
[26] Y. Nishida, K. Nakane, T. Satoh, J. Power Sources 68 (1997) 561.
[27] J. Kim, K. Amine, J. Power Sources 104 (2002) 33.
[28] R. Koksbang, J. Barker, H. Shi, Y. Saidi, Solid-State Ionics 84 (1996) 1.